Modeling of Fault Reactivation and Induced Seismicity During Hydraulic Fracturing of Shale-Gas Reservoirs

Jonny Rutqvist*, Antonio P. Rinaldi, Frédéric Cappa, George J. Moridis

Lawrence Berkeley National Laboratory
Earth Sciences Division, Berkeley, CA 94720, USA

* Corresponding author. *E-mail address:* Jrutqvist@lbl.gov (J. Rutqvist)

This report has been published in *Journal of Petroleum Science and Engineering*, 107, 31–44 (2013), and is viewable on line at:
http://www2.epa.gov/sites/production/files/2013-12/documents/fault-reactivation.pdf

ABSTRACT

We have conducted numerical simulation studies to assess the potential for injection-induced fault reactivation and notable seismic events associated with shale-gas hydraulic fracturing operations. The modeling is generally tuned towards conditions usually encountered in the Marcellus shale play in the Northeastern US at an approximate depth of 1500 m (~4,500 feet). Our modeling simulations indicate that when faults are present, micro-seismic events are possible, the magnitude of which is somewhat larger than the one associated with micro-seismic events originating from regular hydraulic fracturing because of the larger surface area that is available for rupture. The results of our simulations indicated fault rupture lengths of about 10 to 20 m, which, in rare cases can extend to over 100 m, depending on the fault permeability, the in situ stress field, and the fault strength properties. In addition to a single event rupture length of 10 to 20 m, repeated events and aseismic slip amounted to a total rupture length of 50 m, along with a shear offset displacement of less than 0.01 m. This indicates that the possibility of hydraulically induced fractures at great depth (thousands of meters) causing activation of faults and creation of a new flow path that can reach shallow groundwater resources (or even the surface) is remote. The expected low permeability of faults in producible shale is clearly a limiting factor for the possible rupture length and seismic magnitude. In fact, for a fault that is initially nearly-impermeable, the only possibility of larger fault slip event would be opening by hydraulic fracturing; this would allow pressure to penetrate the matrix along the fault and to reduce the frictional strength over a sufficiently large fault surface patch. However, our simulation results show that if the fault is initially impermeable, hydraulic fracturing along the fault results in numerous small micro-seismic events along with the propagation, effectively preventing larger events from occurring. Nevertheless, care should be taken with continuous monitoring of induced seismicity during the entire injection process to detect any runaway fracturing along faults.

1. Introduction

The shale gas revolution in the United States has changed the gas industry greatly, through the development and application of innovative completion techniques, including horizontal drilling, massive stimulation of gas-bearing shales by hydraulic fracturing, and micro-seismic monitoring of stimulation. In fact, the two main enabling technologies that have made gas shale plays (representing ultra-low permeability reservoirs) economically viable are: (i) extended-reach horizontal drilling and (ii) multistage hydraulic fracture stimulation (Alexander et al. 2011). Since about 2000, when the Barnett play (and production) in Texas began to develop in earnest, the United States has seen several other important shale plays develop, including the Marcellus, Haynesville and Eagle Ford shales. Meanwhile, shale-gas exploration has gone global, with targets being identified and drilled in Canada, Poland, China and elsewhere. As a result, gas production from shales is being touted as a geopolitical game-changer, a means to reduce greenhouse gas emissions (by being

environmentally more benign in terms of CO_2 production than the coal it intends to replace), a transition fuel, but also as a danger to the environment (Hart et al., 2011).

Concerns have been raised relating shale gas development to a range of local environmental problems, generating a public backlash that threatens to bring production to a halt in some regions (Zoback et al. 2010; Arthur et al. 2008). One concern (that has been dismissed by industry experts as a very remote possibility) is whether hydraulic fracturing could propagate upwards through the overburden and into shallow groundwater aquifers and thereby allow for contamination of potable groundwater resources by escaping hydrocarbons and other reservoir fluids that ascend through the subsurface (Zoback et al. 2010; Arthur et al. 2008). A recent review by Fisher and Warpinski (2011) of field data from thousands of stimulation operations conducted at depths spanning from 900 to 4300 m (3000 to 14000 feet) shows how the monitored injection-induced seismicity occasionally can travel upwards thousands of feet (several hundred meters), but is still confined in the subsurface several thousand feet below potable groundwater resources. In most cases such upward migration of induced seismicity has been associated with fracturing along subvertical faults (Fisher and Warpinski, 2011). Recently, the presence of faults and the potential for reactivation of faults and potential earthquakes have received increasing attentions of shale gas stake holders and the general public.

In this paper we focus on the potential for injection-induced fault reactivation and we also investigate notable seismic events associated with shale-gas hydraulic fracturing. It is clear that native faults can have a significant impact on the hydraulic fracturing operation, but we address the question of whether such activities can cause a notable seismic event (i.e., one that would be felt by the local population). We also investigate the critical parameters affecting fault reactivation, the circumstances under which a substantial fault reactivation can occur, and the conditions under which such a reactivation could create new flow pathways for upward gas migration. Our numerical study of these issues involves coupled fluid flow and geomechanical modeling, linked with seismological theories. The modeling is generally tuned towards conditions usually encountered in the Marcellus shale play in the Northeastern US at an approximate depth of 1500 m (~4,500 feet). Our simulation results indicate (a) that the possibility of hydraulically-induced fractures for shale stimulation causing activation of faults and new flow paths that can reach shallow groundwater resources (or even the surface) is remote, and (b) that shale gas hydraulic fracturing operations might only give rise to micro-earthquakes, consistent with field observations to date (Fisher and Warpinski (2011).

2. Potential fault reactivation issues

The potential for injection-induced fault reactivation associated with shale gas hydrofracturing and other industrial underground injection activities is an important issue, not just from a safety viewpoint, but also from a public acceptance perspective (Kerr, 2012). A shale-gas fracturing campaign might take place in a relatively confined rock

volume, in tight rock, and carried out in a number of sequential stages, in which one stage could involve injection of half a million gallons of water for a few hours (DOE, 2009). Evidence of injection-induced shear reactivation along minor faults within shale plays has been indicated by Das and Zoback (2011), but these are local events of very small magnitude, i.e. -2 to -3. In fact, it is most likely that shear reactivation of pre-existing fractures and minor faults within the shale play are instrumental to increasing productivity (Zoback et al., 2012). Moreover, micro-seismic events of magnitude -2 to -3, although abundant during stimulation operations, are so small that they would represent shear along fractures a meter or less in diameter, but may be spaced hundreds of meters apart. Still, substantial increases in permeability and productivity could occur as a result of the stimulation, indicating that aseismic shear slip might be important for enhancing permeability and production (Zoback et al,. 2012).

Analogously, aseismic reactivation may also play a role in enhancing permeability along subvertical faults that might extend upwards from the shale play. Another question is whether fracturing of gas-bearing shales could provide sufficient energy to create a seismic event that would be sufficiently large to be felt by the local population. Thus, while abundant micro-seismic events of such low magnitude that are undetectable by humans are an integral part (and are routinely used for monitoring) of the shale-gas fracturing operations, notable seismic events may only be possible to occur at some specific sites, related to local structural geology, stress conditions, rock-mass properties (e.g., soft and ductile vs. hard and brittle, or fractured), and depending on injection operational practices and parameters. One of the objectives of our study is to determine the conditions that could produce substantial fault reactivation, and the corresponding potential consequences.

It is known that faults can affect hydro-fracturing operations both in shale gas and tight-sand gas, including hydraulic stimulations channelized to propagate along faults (Husley et al., 2010; Alexander et al., 2011; Fisher and Warpinski, 2011). As a result, a fault can effectively dominate the fracture growth and redirect all the energy of the treatment into the fault system and out of the target zone (Alexander et al., 2011). Analyzing the monitoring of thousands of shale-stimulation operations in US major shale plays, Fisher and Warpinski (2011) showed how the monitored injection-induced seismicity can occasionally travel upwards thousands of feet (several hundred meters), in most cases caused by inducing fracturing along faults. In these cases, the upward limits of the observed induced micro-seismicity were found to be limited to several thousand feet below the potable water aquifers, and the magnitudes of the events were small. Thus, field observations to-date show that although fluids can migrate several thousand feet along a fault, they tend to cause local micro-seismic events perhaps along oblique fracturing in the fault damage zone, rather than one larger-scale reactivation event along the entire fault plane (Husley et al., 2010).

Recently, a few cases have been reported in which shale gas stimulation has been associated with larger-than-usual shale-gas seismic events. One such case occurred in 2011 near the Preese Hall well site in Lancashire County, near Blackpool, UK, where two seismic events of magnitude 2.3 and 1.5 were observed (de Pater and Baisch, 2011). Site

investigation of this case indicated that the seismicity was likely induced by direct injection of a high percentage of the injection fluid into a fault zone that had not been previously mapped and which does not extend to the surface (de Pater and Baisch, 2011). The investigators estimated that the injected fluids migrated as much as 2000 ft (~600 m) upward along the fault. In another case, the Oklahoma Geological Survey (OGS) recently investigated possible shale-gas-related seismic events induced by hydraulic fracturing that occurred in January 2011 in the Eola Field of Garvin County, Oklahoma. There was a clear temporal correlation between the time of stimulation and the occurrence of forty-three earthquakes that ranged in magnitude from 1.0 to 2.8, all within about 24 hours of a vertical gas well stimulation. Moreover, the earthquake hypocenters were located (with considerable uncertainty) within 5 km from the injection well, and at a depth ranging from 1 to 6 km. The OGS found that the temporal and spatial correlation of stimulation and the earthquakes, along with a reasonable fit to a simple physical model of pressure diffusion, suggested the possibility that the earthquakes were induced by the hydraulic-fracturing operation (Holland, 2011).

The maximum magnitudes reported in the above cases, i.e. 2.3 and 2.8, can still be classified as micro-seismicity. According to the US Geological Survey's classification, these are very minor events with an estimated annual worldwide occurrence of about 1,300,000 times (Table 1). Depending on factors such as the distance to hypocenter and the ground conditions, the strength of ground shaking (i.e., the intensity) of such a low magnitude event may not be sufficient to be perceived by humans. A magnitude 3 to 4 event occurring in the shallow crust, e.g., at a depth of a few km, would most likely be felt by humans near its epicenter. One of the goals with this study is to use numerical modeling to investigate whether, and under what conditions, such a notable event could be produced during a shale-gas hydraulic fracturing operation.

3. Model for analyzing potential fault reactivation

In this section we discuss the model we used to analyze the potential for fault reactivation and the associated seismic magnitude. We used a coupled multiphase flow and geomechanical numerical model to calculate the fault responses, and applied seismological theories to estimate the corresponding seismic magnitude. The modeling is generally tuned towards conditions usually encountered in the Marcellus shale play in the Northeastern US at an approximate depth of 1500 m (~4,500 feet). This includes model input of in situ stress, fluid pressure, temperature, material properties, and injection rates, consistent with the conditions at areas where the Marcellus shale play is located at a depth of about 1500 m.

3.1 Numerical model and conditions

The simulations were performed using the coupled thermo-hydro-mechanical simulator TOUGH-FLAC, (Rutqvist et al., 2002; Rutqvist 2011), which is based on linking the

TOUGH2 multiphase flow and heat transport simulator (Pruess et al. 2011) with the FLAC3D geomechanical simulator (Itasca, 2009). TOUGH-FLAC has previously been applied to the study of fault instability processes on a larger scale, in problems related to multiphase fluid flow and crustal deformations, and CO_2 sequestration (Rutqvist et al., 2007; Cappa et al., 2009; Cappa and Rutqvist, 2011a; 2011b; 2012; Mazzoldi et al., 2012). The fault was modeled as a discrete feature using finite thickness elements having anisotropic elasto-plastic properties, such that shear failure could occur along the fault. It is a so-called *ubiquitous joint* model, in which the fault zone is intensively jointed along a direction parallel to the fault plane. Elasto-plastic properties were defined for both the matrix and the joints within the fault zone (Itasca, 2009). We used a Mohr-Coulomb model with strain softening frictional strength properties, consistent with a seismological slip-weakening fault model. This allowed us to model sudden (seismic) slip events and to estimate their seismic magnitude.

The model domain and the material properties are presented in Fig. 1 and Table 2, respectively. We consider that fractures induced by a hydraulic fracturing operation extend and connect with the fault plane, thereby providing fluid and increasing the fluid pressure within the fault plane (Fig. 1a). Our model domain was discretized into a two-dimensional (2D) plane strain grid (2 km × 2 km in size), representing a cross section across the fault and the hydraulic fractures (Fig. 1b). The system we modeled extended vertically from 500 m to 2500 m in depth, was representative of the Marcellus play with a 30 m thick gas-bearing shale that was bounded at the top and bottom by other low-permeability formations (such as inorganic gray shale and lime stone). This multilayer system is intersected by a pre-existing normal fault with a dip angle of 80° and a length of 1 km. We assume a homogenous distribution of material properties, meaning that the 30 m thick Marcellus gas-bearing shale layer has the same mechanical and hydraulic properties as the adjacent (overlaying) gray shale and intermittent limestone layers. We considered a fault length of 1 km because reactivation of such a fault had the potential to result in a notable seismic event, e.g., a magnitude 4 event. Such a fault might have an initial offset displacement of up to 10 m, and could be up to several meters thick, including the fault core and the adjacent damage zone (Mazzoldi et al., 2012).

The initial conditions included a hydrostatic pressure gradient (9.81 MPa/km) and an atmospheric pressure of 0.1 MPa at the ground surface. Constant pressure and temperature conditions were assumed at the boundaries, except for the left boundary, where no flow occurred. That is, the other boundaries were open for fluid flow. The simulations were conducted in an isothermal mode, which implies that the thermal gradient was maintained unaltered from the initial conditions during the course of the simulation. Null displacement conditions were set normal to the left and bottom boundaries, whereas constant stress was imposed normal to the right and top boundaries (Fig. 1b).

One of the most important parameters related to the potential for fault reactivation is the in situ stress field. In general, the stress field in the Northeastern United States, including the lower Devonian shales of the Appalachian Plateau, is strike-slip (Evans et al., 1989; Evans, 1989). This means that the maximum and minimum compressive principal stresses, σ_1 and

σ_3, are horizontal, and the intermediate principal stress, σ_2, is vertical. Hence, $\sigma_H > \sigma_V > \sigma_h$, where σ_H and σ_h are the maximum and minimum compressive horizontal stresses, and σ_V is vertical stress. However, at greater depths, such as the deepest parts of the Marcellus shale, the vertical stress may become the maximum principal stress. In our study, we consider the minimum principal stress to be horizontal and directed parallel to the horizontal producing well, leading to vertical hydro-fractures perpendicular to the well as shown in Fig. 2. This is also the preferred and most common well configuration in the field (Alexander et al., 2011). In our simulations, the fault was subvertical, dipping at an angle of 80°, and was assumed to strike normal to the minimum principal stress (Fig. 1).

We set the vertical stress gradient (maximum principal stress) to 26,487 Pa/m, corresponding to an overburden density of about 2700 kg/m^3. This gradient was obtained from Starr (2011) who estimated the overburden vertical stress based on measured density of all the overburden layers above the Marcellus shale. Several sources (e.g. Cippolla et al., 2010) indicate a closure stress of about 0.7 psi/ft and this corresponds to a minimum horizontal compressive stress gradient of 15,834 Pa/m across the Marcellus shale. Additionally, this corresponds to a horizontal-over-vertical stress ratio of $R = \sigma_h/\sigma_V = 0.6$. As shown in Fig. 1b, this means that we apply a stress gradient of minimum compressive horizontal stress of $\sigma_h = 0.6\sigma_V$ on the left lateral boundary of the model. The value of the maximum principal compressive stress (also maximum horizontal compressive stress) does not have an impact on the potential for reactivating the subvertical fault because the maximum principal compressive stress is in a direction normal to our 2D model (i.e. parallel to the strike of the fault). The horizontal over vertical stress ratio is, on the other hand, a critical parameter; in our study it varied between 0.5 and 0.7.

We assigned to the fault a coefficient of friction of 0.6, with a residual value (after slip) equal to 0.2. This reduction of coefficient of friction with shear allowed us to simulate sudden (seismic) shear slip and to estimate the seismic magnitude. A larger difference between the peak and residual friction values represents a more brittle behavior that could lead to seismic event, whereas a friction angle unaffected by shear strain would represent ductile behavior leading to an aseismic slip. A coefficient of 0.6 is commonly observed for laboratory samples as a lower limit value for the most common rocks and has also been inferred from field observations as the earth's shallow crust being critically stressed for frictional failure (Zoback, 2007). However, clay rich fault rock could have a much lower coefficient of friction, especially under wet conditions (Zoback, 2007; Samuelson et al., 2012). A residual shear strength of 0.2 is not unusual for clay rich fault gauge (Ikari et al., 2009). However, a complicating factor is that we should relate our residual coefficient of friction to the dynamic friction coefficient in seismology, which depends on displacement rate among other factors (Samuelson et al., 2012). Consequently, we varied these parameters in the simulations.

Gas-bearing shale plays that are most suitable for gas extraction tend to be brittle, allowing for hydraulic fracturing. As such, a Young's modulus of 30 GPa and a Poisson's ratio of 0.2 were assigned to the base case in our study. To our knowledge, there are no published

data on laboratory-determined static Young's modulus and Poisson's ratio for the Marcellus shale. Thus, in our investigation we assigned average values and ranges obtained from laboratory tests on Barnett Shale (Tutuncu, 2010) because of the similarities between the Marcellus and the Barnett shales in terms of porosity, clay content and total organics content.

Considering that the fault zone is defined as a zone that could be several meters thick and intensively jointed, our initial approach was to assign to it a zero cohesion and softer elastic properties than the surrounding, more competent, shale. We set the Young's modulus for the fault rock to 5 GPa, representing a significant reduction from the 30 GPa value for the surrounding shale (Fault 1 in Table 1). As shown by the simulation results discussed later, this is a valid approach for modeling the injection-induced opening of pre-existing joints and the subsequent fault reactivation by shear. However, to consider the effects of fracture propagation along the fault, we had to assign stiffer elastic properties to the fault that had to be comparable to the stiffness of the surrounding shale host rock (Fault 2 in Table 1). Moreover, we assigned an initial cohesion of 3 MPa that was reduced as a function of strain upon fracturing or shear using a strain-softening formulation. This was necessary because, for a soft intensively jointed fault rock with Young's modulus of 5 GPa, poro-elastic stress within the fault effectively prevented fracturing from occurring before shear reactivation.

The permeability of the fault is also expected to be important for the potential of fault reactivation. Consequently, we conducted a sensitivity analysis by varying this parameter as well. The permeability of the shale was set to 10^{-19} m^2, whereas the permeability of the fault was varied from 10^{-19} m^2 (nearly-impermeable base case) to 10^{-16} m^2, the latter case representing potential permeability along a thin damage zone of the fault. The assumption of an initial impermeable fault (hydraulically indistinguishable from the host rock) is a realistic base case. A relevant example is a fault zone in the Opalinus shale exposed at the Mont Terri Rock Laboratory, Switzerland (Croisé et al., 2004). This zone is several meters thick, has an inferred shear offset of 5 m, but is hydraulically indistinguishable from the host rock, having an estimated permeability $k = 2\times10^{-20}$ m^2 (Croisé et al., 2004). Thus, although intensively fractured, it is practically impermeable, because the fractures are completely sealed.

Fault activation can induce changes in permeability along the fault as a result of shear dilation and damage. In this study, we first used a permeability change model based on porosity being a function of volumetric strain (the sum of elastic and plastic volumetric strain). This model had been previously applied to fault studies by Cappa and Rutqvist (2011b), and is described by the following equation:

$$\phi = 1 - (1 - \phi_i)e^{-\varepsilon_v} \quad (1)$$

$$k = k_i\left(\frac{\phi}{\phi_i}\right)^n \quad (2)$$

Equation (1) and (2) was originally developed and applied by Chin et al. (2000) for modeling the permeability evolution in petroleum reservoirs undergoing irreversible (plastic) mechanical changes. Indeed, relating the permeability to porosity and volumetric

strain (rather than stress) enables consistent permeability correction for both elastic and plastic mechanical behavior. Equation (1) was derived by Chin et al. (2000) for coupled fluid flow and geomechanical governing equations along the lines of Biot's self-consistent theory and conservation principles, and assumes incompressible grains (Biot's $\alpha = 1$). Equation (2) is an empirical function that is phenomenologically developed from laboratory and/or field measurements and has been shown to be widely applicable to geological materials (Wong et al., 1997).

The empirical coefficient n in Equation (2) characterizes the porosity sensitivity of permeability. In consolidated geological materials n has values ranging from 3 up to 25 (Wong et al., 1997; David et al. 1994). In this study, following Cappa and Rutqvist (2011b), a value of n = 15 was used in the simulations. This was consistent with the value originally assumed by Cappa and Rutqvist (2011b) in their study of permeability changes with fault reactivation, resulting in a permeability enhancement by about 2 orders of magnitude upon complete fault shear activation.

The final permeability enhancement upon shear activation depends on the total shear strain and shear dilation and consequently the value of the dilation angle applied to the elasto-plastic model. In this study the dilation angle was set to 10° (Table 1) assuming somewhat brittle and dilatant mechanical behavior. A 2 orders of magnitude increase in fault permeability upon reactivation is reasonable in relatively stiff shale suitable for hydraulic fracturing stimulations. Such permeability increases upon reactivation have been inferred from natural analogues associated with fault valve behavior in naturally overpressured reservoirs (Poston and Berg, 1997; Sibson, 2003), and play an important role related to gas trapping for hydro-carbon reservoirs (Nygård et al, 2006: Ingram and Uril, 1999).

However, as shown by Cappa and Rutqvist (2011a, b), while the initial permeability had some effect on the fault activation results, the shear-induced permeability changes along with the activation had a negligible impact on the size of the rupture and the moment magnitude. Mazzoldi et al. (2012) showed how the initial fault permeability could play a role on the pressure evolution, but also indicated that, as soon as the critical pressure to activate the sudden slip was reached, the permeability did not affect (or only slightly affected) the resulting slip and rupture.

In the case of hydraulic fracturing along the fault plane, a fracture permeability model based on fracture aperture was applied (Rutqvist et al., 2012). According to this fracture permeability model, fluid may not permeate into the fracture until a certain threshold crack opening displacement (COD) is achieved. We estimated the COD from the strain normal across the fault, assuming that when tensile failure occurs, the normal strain within the fault is localized, resulting in the opening of one single or multiple parallel fractures according to:

$$b_m = B \times \varepsilon_n \tag{3}$$

where b_m [m] is the mechanical aperture, equivalent to the COD [m], and B [m] is the element width across the fault (or the fracture spacing in case of multiple parallel fractures). According to Rutqvist et al., (2012), we calculated changes in the equivalent permeability resulting from crack opening as being superimposed on the initial (intact) rock permeability according to:

$$k = k_0 + k_f = k_0 + A\left(\varepsilon_n - \varepsilon_n^t\right)^3 \tag{4}$$

where k_0 [m^2] is the initial (intact) rock permeability, A [m^2] is a constant, and ε_n^t [-], is the threshold strain related to the COD (or b_m) threshold for the onset of permeability changes. For a threshold COD or threshold aperture b_m^t of about 100 to 200 μm, and for B = 2.5 m, the threshold strain across and normal to the fault ε_n^t is estimated to be on the order of 10^{-4}. In the simulation we set $A = 10^{-5}$ m^2 meaning that the permeability would increase to about 10^{-14} m^2 for a plastic strain normal to the fault on the order of 10^{-3}. We estimated this to be at the low end of the possible permeability change due to fracturing, but this was still sufficient to provide rapid pressure diffusion in the fractured elements along the fracture propagation.

For our 2D analysis, we simulated the water injection during stimulation as representatively as possible of conditions during hydraulic fracturing operations in the Marcellus shale. Generally, shale gas stimulation requires a large volume of injected water to attain hydraulic fracturing. The water volume may exceed 500,000 gallons at each stage of hydraulic fracturing along a horizontal well bore (US DOE, 2009). Typically, each stage is characterized by a sub-stage sequence, during which water is pumped at a rate of 3000 gal/min (about 200 kg/s) for a few hours. In this study, we considered the effects of an injection stage that creates a fracture that breaks into a fault zone. From the total amount of water injected in a typical stage we estimated the injection rate into our 2D simulation grid as follows: A wellbore is often 1000 to 2000 m long, and the hydraulic fracturing process may involve 10 to 20 stages. We thus assumed that each stage affected a length of about 100 m along the horizontal wellbore. Micro-seismic events observed at shale gas production sites appear to indicate that the producing zone extends 300-500 ft (about 100 m) along the vertical direction, and the lateral extent is about 1000-1500 ft (about 300 m) (Fig. 2). Thus, using these parameter estimates, we assumed an injection rate per volume unit during a single stage of $200/(100\times100\times300) = 6.6\times10^{-5}$ kg/s/m^3, which corresponded to an injection rate of about 10^{-4} kg/s into a 1.25 m^3 grid-block. Again, we assume that fracturing from the stimulation intersects the fault and in the model simulation we therefore inject this amount of fluid into a few numerical gridblocks within the fault in the injection point shown schematically in Fig. 1.

The injection rate of 10^{-4} kg/s per element at the intersection of the stimulation zone and the fault in our 2D model is a rough estimate for a 200 kg/s injection in a full 3D field setting. Most important in this study is the resulting time evolution of fluid pressure at the injection

point, which in this case represents the intersection of the hydraulic fractures (or stimulation zone) with the fault plane (Fig. 1). In the 2D model, we represent the evolution of the reservoir pressure within the 100×100×300 m^3 stimulated volume and how this pressure would evolve at the intersection between the stimulation zone and the fault. In a field setting, the fluid pressure is expected to increase to maximum pressure within a few hours of injection for one stimulation stage. The maximum pressure will be limited by the fracturing pressure (just above the magnitude of the minimum compressive principal stress), but if a very permeable fault, the injection pressure may remain low as a result of pressure release through the fault.

Due to the difficulty of estimating a representative injection rate in our 2D model, we apply different approaches for applying the injection rate, not always fixing the rate at 10^{-4} kg/s per fault injection element. For example, in some sensitivity analyses we apply an injection rate that would result in a similar pressure build up in a steady pressurization, e.g. reaching a pressure just above the minimum compressive principal stress within about 3 hours. Using this approach we let the simulation decide what injection rate is required to match such a pressure evolution. The injection rate will depend on how much fluid the fault can accommodate for a given pressure evolution at the intersection between the stimulation zone and the fault. This in turn, will depend on the faults initial permeability and how much permeability will change as a result of reactivation. Finally, in one case we inject at such a high rate that pressure increases to maximum pressure corresponding to fracture initiation pressure within about 15 minutes from the start of the injection. Thus, our analysis covers a wide range of injection scenarios, including constant rate and constant pressurization rates with time to peak pressure ranging from 15 minutes to several hours.

3.2 Estimating seismic magnitude

Following the approach in Cappa and Rutqvist (2011a) and Mazzoldi et al. (2012), the seismic magnitude is estimated using seismological theories. First we quantify the overall size of a simulated seismic event based on the seismic moment M_0, which, for a ruptured patch on a fault, is defined by Kanamori and Brodsky (2001) as:

$$M_0 = \mu A d \tag{6}$$

where μ is the shear modulus [Pa], A is the rupture area [m^2], and d is the mean slip [m]. Then the moment magnitude (M) of an earthquake, in terms of seismic moment, is given by Kanamori and Anderson (1975) as

$$M = (\log_{10} M_0 / 1.5) - 6.1 \tag{7}$$

where the seismic moment, M_0 , is in Nm. Thus, in the modeling we need to distinguish between (a) the co-seismic fault slip and surface area, which occur during the sudden slip event, and (b) the aseismic slip, which may be much larger, but occurs after the co-seismic slip. For simplicity, when estimating the seismic moment according to Equation (6), we assume a circular rupture patch with a diameter equal to the calculated rupture length in our 2D model.

4. Simulation results

Here we discuss the simulation results for 3 distinct cases. In the first case, we present results associated with a variable injection rate. The rate was designed to achieve a steady rate of pressure increase and to attain a maximum pressure of about 30 MPa in 3 hours. In the second case, we present results for a constant rate of injection, which was maintained unaltered regardless of fault permeability, actual pressure evolution, and duration of the injection stage. The properties of Fault 1 in Table 1 were used for these simulations. In the same case, we also conducted parametric studies of sensitivity analysis to identify crucial parameters and their effect on a potential fault reactivation. Finally, in the third case we discuss the results stemming from hydraulic fracturing along the fault with intermittent shear activation using the properties of Fault 2 (Table 1).

4.1 Variable injection rate and a steady pressurization rate

Fig. 3 shows the simulation results for the base case stress field, in which the horizontal stress is 0.6 times the vertical, and which involves an injection rate that would result in a pressure approaching 30 MPa in about 3 hours. The fault permeability was varied between 10^{-19} and 10^{-16} m^2. The 2D modeling injection rate into the fault varied from a minimum of about $Q = 10^{-4}$ kg/s (which according the Section 3.1 correspond to 3D field scale injection rate of about 200 kg/s) in the case of a nearly-impermeable fault ($k = 10^{-19}$ m^2), up to a maximum of about $Q = 3.5\times10^{-3}$ kg/s (corresponding to 700 kg/s 3D field scale rate) in the case of a relatively permeable fault ($k = 10^{-16}$ m^2). In a field setting, the injection rate would probably no be as high as 700 kg/s as the field operator would probably suspect leakage and this high rate might also exceed maximum pump capacity. However, we still apply this rate for a comparison of the fault responses under a given steady pressurization rate.

As shown in Fig. 3, in all cases the pressure increased gradually during the injection process. In the case of an initially nearly-impermeable fault, the pressure increased until it reaches the pre-set maximum pressure of 32 MPa, but no reactivation occurred. In fact, the simulation showed that the very localized injection that takes place over the thickness of the fault resulted in poro-elastic stresses (i.e., increases in the total stress near the injection point) that effectively prevented shear failure (and fracturing) along the fault.

The resulting seismic magnitudes associated with fault ruptures are dependent on the rupture length and by the depth of penetration of the fluid pressure into the fault before the rupture occurs. In the case of low fault permeability, i.e., when $k =10^{-19}$ and $k =10^{-18}$ m^2, no reactivation or seismic events were observed because the fluid pressure did not penetrate the fault sufficiently during the 3 hour-injection period. For a higher initial permeability of the fault (i.e., when $k =10^{-17}$ and $k =10^{-16}$ m^2), a more significant amount of fluid was shown to penetrate into the fault, which then opens up mechanically by the rising internal pressure. The permeability of the fault increased with the reduction in the effective stress and the

opening of pre-existing fractures within the fault, therefore the pressure never reached 32 MPa. However, the pressurization along the fault also lowered the shear strength, and consequently a shear slip event occurred at the end of the 3 hours injection. For example, in the case of the fault $k = 10^{-17}$ m^2, a small seismic event was observed along an approximately 9 m-long section of the fault. The seismic slip event is identified as the sudden shear slip in the mid right graph in Fig. 3. The panels in the bottom of Fig. 3 show the rupture lengths along which shear failure occurred for the various fault permeability values we investigated. The largest rupture length (23.5 m) corresponded to the highest fault permeability ($k = 10^{-16}$ m^2). As a result of the associated larger rupture area, the seismic magnitude increased, but still represented a very small seismic event of magnitude less than 1 that would only be detectable by geophones, and which would not be discernible by humans.

4.2 Constant rate injection

Fig. 4 presents the simulation results of the second case we studied, which involved a fixed injection rate (about $Q = 10^{-4}$ kg/s per fault injection element) regardless of the varying fault permeability ($k = 10^{-19}$ m^2, 10^{-18} m^2, and 10^{-17} m^2). Recall from Section 3.1 that the 10^{-4} kg/s 2D fault element injection rate would mimic a 200 kg/s injection rate in a full 3D field scale setting. For this constant rate injection, the injection was ceased when the pressure reached 32MPa (usually in 3 hours in the case of nearly-impermeable fault, as indicated in the previous section), or when failure occurred (about 3 days and 7 days for $k = 10^{-18}$ m^2 and 10^{-19} m^2, respectively). The resulting seismic magnitudes were as small as in the previous case (discussed in Section 4.1), and were controlled by the rupture length and by the depth of penetration of the fluid pressure into the fault before the onset of rupture. The results in the case of low permeability ($k = 10^{-19}$ m^2) were the same as the previous case: no reactivation or seismic events were observed because the fluid pressure did not penetrate sufficiently into the fault in the 3 hours of injection. When the initial permeability of the fault was higher (i.e., when $k = 10^{-18}$ m^2 and $k = 10^{-17}$ m^2), the fluid penetrated the fault and a slip fault reactivation of low magnitude occurred, the largest of which resulted in a rupture length of about 90 m, and with a corresponding seismic magnitude of 1.73, after 7.5 days of continuous injection at $Q = 10^{-4}$ kg/s. When the fault permeability was assumed to be higher than $k = 10^{-17}$ m^2, it was not possible (for the selected Q) to increase the fluid pressure sufficiently to create any shearing because the fluid easily spread out within the fault, and the corresponding pressure dissipated rapidly. To increase pressure sufficiently to cause shear activation would require much higher injection rate and such a case was presented in Section 4.1 above for fault permeability as high as $k = 10^{-16}$ m^2.

It is interesting to compare the two cases in Figs. 3 and 4 that correspond to a fault permeability of $k = 1\times10^{-17}$ m^2. These involve different injection rates and times, and the time to fault reactivation is different. For a lower injection rate (Fig. 4), it takes longer for the actual rupture to occur, but at that time a larger area of the fault has been pressurized and, therefore, a larger area of the fault is ruptured. This indicates that a slow pressure build up along a permeable fault might be more likely to cause larger seismic events, whereas a rapid pressure build up would be more likely to cause smaller localized events.

However, a continued pressurization of the fault after the first event might also cause repeated smaller events by rupturing additional parts of the fault.

4.3 Effect of in situ stress field

Fig. 5 shows the results for the case of a nearly-impermeable fault—i.e. a fault that has the same permeability as the host rock—subjected to different regimes of horizontal over vertical stress ratio R. The injection rate was constant at $Q = 10^{-4}$ kg/s, which according to Section 3.1 would correspond to a 200 kg/s injection rate for one stimulation stage in a full 3D field setting. When R is very small, e.g. $R = \sigma_h/\sigma_V = 0.5$, the fault is practically critically stressed for slip even initially, i.e., before the onset of injection. The critically stressed conditions is shown in Fig. 5 lower panel where in the case of $R = 0.5$, the dashed (red) line representing shear strength is on top of the solid (red) line representing shear stress, and thus the shear stress is equal to shear strength. Under these conditions, if the residual friction angle is assumed to have a value of 0.2, the bedrock could not sustain the in situ stress field and the entire fault would reactivate. Therefore, in the simulation cases in Fig. 5, the coefficient of friction remains constant at 0.6 and we obtain gradual (aseismic) slip during the course of the injection. The slip during the first 3 hours was negligible (see upper left panel in Fig. 5); continuing injection would be expected to result in a more significant shear. Still, even in the case of the most unfavorable stress ratio of $R = 0.5$, the fault slip after 1 day was limited to 20 m, and slip displacement was less than 0.0005 m.

For completeness in the comparison, and for the sake of investigating circumstances that could cause a more substantial slip, we investigated the effect of unfavorable stress ratios R in a more permeable fault, i.e., one with $k = 10^{-16}$ m^2 (Fig. 6). In this case, when the fault was initially critically stressed fault (with $R = 0.5$), the fault slip was triggered immediately upon the onset of injection and it progressed continuously during the 3 hour injection, causing aseismic shear slip along an 850 m-long section of the fault. During the 3 hour injection period, the fluid pressure penetrated only about 35 m into the formation, yet over 800 m of the fault experienced aseismic fault slip. This shows that more substantial slip and rupture can be induced when a fault is (a) initially near critically stressed and (b) sufficiently permeable to allow significant fluid penetration into the fault. Under these conditions, the fault was already relatively permeable before the beginning of the injection, and the aseismic slip did not increase its permeability much further.

4.4 Effects of fault properties

Recognizing the uncertainties in assigning fault properties, we conducted a sensitivity analysis study to investigate the effects of fault properties on the estimated rupture length and seismic magnitude. We determined that the dilation angle had no significant impact on our results if varied between 0 and 20°. (We do not show the simulation results for a dilation angle 0 and 20°, because they are almost identical to those shown for a 10° dilation angle in all cases). However, as shown in Fig. 7, the residual friction angle has a significant impact on the rupture length and the seismic magnitude. A reduction in the residual friction angle from 20° to 11° (i.e. a reduction in residual coefficient of friction from 0.36 to 0.2) resulted in an increase of seismic magnitude from 0.15 to 0.72, i.e., an increase in the

seismic magnitude by a factor of 5, but still remaining at the micro-seismic level that can only be detected by geophones and are imperceptible by humans. In our study, the peak friction angle was set to 31° (coefficient of friction 0.6), whereas in the base case the residual friction angle was set to 11° (coefficient of friction 0.2). The shear stress drop associated with loss of friction has a direct impact on the calculated shear displacement which in turn affects the calculated rupture area and seismic magnitude through Equations (1) and (2). For example, in Fig. 7 lower panel we can observe that the shear stress drops most (from about 6 MPa to about 2.5 MPa) resulting in the largest rupture length (23.5 m) and consequently the largest seismic magnitude. Note that we believe that a drop from 31° to 11° in the friction angle is a conservative choice for shale; under realistic conditions, the difference between peak friction angle and residual friction angle is likely to be much smaller and resulting in a much smaller stress drop, leading to even smaller seismic events.

4.5 Constant rate injection and hydraulic fracturing

Finally, we conducted a simulation case in which hydraulic fracturing occurs along the fault. This means that even in the case of an initially impermeable fault, hydraulic fracturing can open up fluid flow paths along the fault, and thereby allow fluid pressure to penetrate along the fault to potentially result in shear reactivation. Here we assumed that the elastic properties of the fault rock are the same as those of the surrounding shale rock, i.e., E = 30 MPa, and ν = 0.2, i.e. according to Fault 2 in Table 1. Thus, in this case we considered a fault zone that is weakened in terms of strength properties, but with an overall mechanical stiffness equivalent to the surrounding shale.

Fig. 8 presents the results of the hydraulic fracturing simulation for three cases of initial fault permeability ($k = 10^{-19}$, 10^{-18}, and 10^{-17} m^2). The injection was localized into a 0.75 m length of the fault at the injection point shown in Fig. 1b. Hydraulic fracturing was observed to initiate in all cases at a well pressure of about 35 MPa (Fig. 8 lower panel). We kept a high injection rate to achieve a pressure needed for hydraulic fracturing (about 35 MPa) during the first minutes (about 15 minutes). As previously, the injection lasted about 3 hours (US DOE, 2009). Note that the permeability function we used in this hydraulic fracturing case permit us to use the same injection rate and to reach about the same amount of overpressure independently from the choice of the initial permeability.

After the first minutes of fast compression, the well pressure fluctuated around the 35 MPa level, signifying fracture propagation through the numerical grid along the fault (Fig. 8 lower panel). In all cases a fracture first propagated about 4 to 8 m before shear became the dominant failure mode. This is shown in Fig. 8 upper panel where the initial fracturing length is seen as an additional permeability enhancement extending up to 8 m around the injection point, whereas the final rupture length indicated by the length of induced permeability changes extends as much as 25 m. This extension of permeability enhancement corresponds to the extension of the zone of plastic strain showing how the plastic strain results a significant permeability enhancements through Equations (1) through (4). Even in the case of the lowest permeability ($k = 10^{-19}$ m^2), the fracturing and associated permeability increase enabled fluid pressure to migrate sufficiently along the fault to

initiate a self-propagating shear rupture that extended outside the pressurized zone. The continuous fracturing resulted in a more continuous shear activation that was taking place in small steps, resulting in very small seismic events of magnitude less than 0 (Fig. 8 mid panel). Only in the case of the highest permeability ($k = 10^{-17}$ m^2) did a relatively large shear activation step occurred at about 2 hours of injection. However, even this amounted to a very small event with an estimated magnitude of 0.38. After the entire 3 hours injection, the rupture length remained limited, not exceeding 25 m.

5. Concluding remarks

We have conducted scoping calculations to study the potential for injection-induced fault reactivation and induced seismicity associated with shale-gas hydraulic fracturing operations. We found that our approach, which involved using the TOUGH-FLAC simulator, representing a fault by finite-thickness numerical elements, anisotropic plasticity, and linkage with seismological theories, is adequate to describe the problem at hand. The approach was tested using a 2D model, broadly representing the conditions at the Marcellus shale play. We conducted the simulations for wide range of fluid pressurization rates using 2D fault-element injection rates, which cover the range of conditions at a real 3D field setting. For example, we covered fluid pressurization times as fast as 15 minutes and as slow as several hours. The simulation results show that the 2D fault-element injection rate depends on how much fluid the fault can accommodate for a given pressure evolution at the intersection between the stimulation zone and the fault. This in turn, depends on the faults initial permeability and how much permeability changes as a result of reactivation. In our simulation, the reactivation could result in a permeability change of several orders of magnitude. However, the results also showed that it is the initial permeability that is most important for the final rupture length and seismic magnitude, whereas the reactivation-induced permeability changed had a relatively small impact on the simulation results. The key is how far the pressure can propagate into the fault, i.e. how much surface area that is exposed to the elevated fluid pressure at the time a sudden slip occurs. In our 2D model representation of this 3D field problem we have been able to capture such key processes and to provide a conservative (high end) estimate of potential rupture length and seismic magnitude.

The results of our study indicate that the hydraulic fracturing stimulation may only give rise to small micro-seismic events, consistent with earlier field observations. That is, when faults are present, somewhat larger seismic events are possible—compared to those associated with regular hydraulic fracturing seismic events—because larger surface areas are available for rupturing. Fault rupture (vertical) lengths of about 10 to 20 m, and in rare cases over 100 m, were observed depending on the fault permeability, the in situ stress field, and the shear strength properties of the fault. The peak and residual coefficients of friction assigned to a fault are important parameters that control the potential seismic magnitude, along with the fault slip weakening. In addition to the single event rupture length of 10 to 20 m, repeated events and aseismic slip were shown to amount to less than

0.01m, with the total length of shear rupture extending up to 50 m. This indicates that the possibility of hydraulically induced fractures at great depth (thousands of meters) causing activation of faults and creation of a new flow path that can reach shallow groundwater resources (or even the surface) is remote.

We found that, in the case of a critically stressed fault that is also permeable, the rupture zone can be more extensive. Much of such displacement seems to be aseismic, progressing continuously during injection. However, an expected low permeability of a fault in gas–bearing shales is clearly a limiting factor in the size of the possible rupture length and the corresponding seismic magnitude. It can be argued that faults in gas-bearing shales are likely to have low permeability, as otherwise the gas would have escaped over geological time. It may also be argued that, if faults were permeable, they would be active, critically stressed, and with a coefficient of friction close to its residual value. In such a case, only aseismic slip might occur and, because of ductile slip, the permeability would not change considerably.

The results we present here are still preliminary, and serve to identify the most important parameters for potential fault reactivation, such as the stress field, and fault properties. In fact, for a fault that is initially impermeable, the only possibility of a larger fault slip event would be opening by hydraulic fracturing, thus allowing pressure to penetrate the matrix. However, our simulation results show that, if the fault is initially impermeable, hydraulic fracturing along the fault results in numerous small micro-seismic events, effectively preventing larger events from occurring. Moreover, in our simulation we assigned homogenous properties along the fault, whereas in the field they could be significantly heterogeneous. That is, the coefficient of friction is likely of vary along the fault, and the fault might first rupture along fault sections of lower strength, perhaps increasing the potential for several smaller events, rather than a few bigger ones. Finally, our 2D representation of the full 3D field setting is a simplification that has an impact on our estimated seismic magnitudes. In the end, the 2D simplification and the use of homogeneous fault properties are likely to result in a conservative (high end) estimate of the fault rupture length and seismic magnitude.

Nevertheless, our simulations to-date illustrate the possibility of fault reactivation once the shear stress exceeds the shear strength and the fault rupture can propagate outside the pressurized zone as a result of the slip weakening the fault behavior. In our studies, we controlled the injection rate such that it ceased when the pressure reached a certain pre-set maximum bottom-hole pressure. In the field it might be difficult to predict the appropriate magnitude of overpressure and, therefore, care should be taken with continuous monitoring of induced seismicity from the start of the injection to detect any runaway fracturing along faults. If large-scale pressurization of faults can be avoided, it is likely that large scale reactivations and notable earthquakes can be avoided altogether. Since aseismic slip might be dominant in the field, the seismic monitoring should, if at all possible, be complemented with deformation monitoring, such as tilt meters. Finally, an adequate site characterization for identifying and avoiding faults should be a priority in any shale gas development.

Acknowledgments

We thank the US Environmental Protection Agency (EPA), Office of Water, for supporting this study under an Interagency Agreement with the US Department of Energy at the Lawrence Berkeley National Laboratory through Contract No. DE-AC02-05CH11231. Technical review by Jihoon Kim, Berkeley Lab is greatly appreciated. The views in this article are those of the authors and do not necessarily reflect the views or policies of the U.S. EPA.

References

Alexander, T., Baihly, J., Boyer, C., Clark, B., Waters, G., Jochen, V., Le Calvez, J., Lewis, R., Miller, C.K., Thaeler, J., Toelle, B.E., 2011. Shale gas revolution. Oilfield Review, Autumn 2011: 40-57.

Arthur, J.D., Bohm B., Layne M., 2008. Hydraulic fracturing considerations for natural gas wells of the Marcellus shale. Presented at the Ground Water Protection Council 2008 Annual Forum, Cincinati, Ohio, USA, 21-24, Sep.

Cappa, F., Rutqvist, J., 2011a. Impact of CO_2 geological sequestration on the nucleation of earthquakes. Geophys. Res. Lett., 38, L17313, doi:10.1029/2011GL048487.

Cappa, F., Rutqvist, J., 2011b. Modeling of coupled deformation and permeability evolution during fault reactivation induced by deep underground injection of CO_2. *Int. J. Greenhouse Gas Control*, 5, 336-346, doi:10.1016/j.ijggc.2010.08.00.

Cappa, F., Rutqvist, J., 2012. Seismic rupture and ground accelerations induced by CO_2 injection in the shallow crust. Geophysical Journal International, 190, 1784–1789.

Cappa, F., Rutqvist, J., Yamamoto, K., 2009. Modeling crustal deformation and rupture processes related to upwelling of deep CO2-rich fluids during the 1965–1967 Matsushiro earthquake swarm in Japan, J. Geophys. Res., 114, B10304, doi:10.1029/2009JB006398.

Chin, L.Y, Raghavan, R., Thomas, L.K, 2000. Fully Coupled Geomechanics and Fluid-Flow Analysis of Wells with Stress-dependent Permeability. SPE Journal 5 (1) Paper 58968, 32-45.

Cipolla, C.L., Lolon, E.P., Erdle, J.C., Rubin, B., 2010. Reservoir modeling in shale-gas reservoirs. Society of Petroleum Engineers (SPE) Reservoir Evaluation & Engineering. August 2010 SPE 125530.

Croisé, J., Schlickenrieder, L., Marschall, P., Boisson, J.Y., Vogel, P., Yamamoto, S., 2004. Hydrogeological investigations in a low permeability claystone formation: the Mont Terri Rock Laboratory. Physics and Chemistry of the Earth 29: 3–15.

Das, I., Zoback, M.D., 2011. Long-period, long-duration seismic events during hydraulic fracture stimulation of a shale-gas reservoir. The Leading Edge, July 2011: 778-786.

David, C., Wong, T.-F., Zhu, W., Zhang, J., 1994. Laboratory measurement of compaction-induced permeability change in porous rock: Implications for the generation and maintenance of pore pressure excess in the crust, Pure Appl. Geophys., 143, 425-456, 1994.

De Pater, C.J., Baisch, S., 2011. Geomechanical study of Bowland shale seismicity. Synthesis Report, November 2011. Cuadrilla Resources Ltd, UK.

Evans, K.F., Engelder, T., Plumb, R.A., 1989. Appalachian stress study. 1 A detailed description of in situ stress variations in Devonian shales of the Appalachian Plateau. Journal of Geophysical Research, 94: 7129-7954.

Evans, K.F., 1989. Appalachian stress study. 3 Regional stress variations and their relation to structure and contemporary techtonics. Journal of Geophysical Research, 94: 17619-17645.

Fisher, K., Warpinski, N., 2011. Hydraulic Fracture-Height Growth: Real Data. paper was prepared for presentation at the SPE Annual Technical Conference and Exhibition held in Denver, Colorado, USA, 30 October–2 November 2011.

Hart, B., Sayers, C., Jackson, A., 2011. An introduction to this special section: Shales. The Leading Edge, March 2011: 273.

Holland, A., 2011. Examination of possibly induced seismicity from hydraulic fracturing in the Eola Field, Garvin County, Oklahoma. Oklahoma Geological Survey Open-File Report OF1-2011.

Hulsey, B.J., Cornette, B., Pratt, D., 2010. Surface Microseismic Mapping Reveals Details of the Marcellus Shale. SPE Eastern Regional Meeting, 12-14 October 2010, Morgantown, West Virginia, USA.

Ikari, M.J., Saffer D.M., and Chris Marone, C., 2009. Frictional and hydrologic properties of clay-rich fault gouge. Journal of Geophysical Research, 114: B05409.

Ingram, G.M., Urai, J.L., 1999. Top-seal leakage through faults and fractures: the role of mudrock properties, Geol. Soc. Spec. Publ., 158, 125–135

ITASCA, 2009. FLAC3D V4.0, Fast Lagrangian Analysis of Continua in 3 Dimensions, User's Guide. Itasca Consulting Group, Minneapolis, Minnesota.

Kanamori, H., Anderson, D.L., 1975. Theoretical basis of some empirical relations in seismology, Bull. Seism. Soc. Am., 65, 1073-1095.

Kanamori, H., Brodsky, E.E., 2001. The physics of earthquakes. Physics Today (June 2001), 34–40.

Kerr, R.A., 2012. Learning how to not make your own earthquakes. Science, 335: 23 March 2012.

Mazzoldi, A., Rinaldi, A.P., Borgia, A., Rutqvist, J., 2012. Induced seismicity within geologic carbon sequestration projects: Maximum earthquake magnitude and leakage potential. International Journal of Greenhouse Gas Control, 10, 434–442.

Nygård, R., Gutierrez, M., Bratli, R.K., Høeg, K., 2006. Brittle–ductile transition, shear failure and leakage in shales and mudrocks, Mar. Pet. Geol., 23, 201–212

Poston, S.W., Berg, R.R., 1997. Overpressured gas reservoirs. Society of Petroleum Engineers, Richardson, Texas.

Pruess, K, Oldenburg. C., Moridis, G., 2011. TOUGH2 User's Guide, Version 2.1, LBNL-43134(revised), Lawrence Berkeley National Laboratory, Berkeley, California.

Rutqvist, J., 2011. Status of the TOUGH-FLAC simulator and recent applications related to coupled fluid flow and crustal deformations. Computers & Geosciences, 37, 739–750.

Rutqvist, J., Wu, Y.-S., Tsang, C.-F., Bodvarsson, G., 2002. A modeling approach for analysis of coupled multiphase fluid flow, heat transfer, and deformation in fractured porous rock, Int. J. Rock Mech. Min. Sci., 39:429-442.

Rutqvist, J., Birkholzer, J.T., Cappa, F., Tsang, C.-F., 2007. Estimating maximum sustainable injection pressure during geological sequestration of CO2 using coupled fluid flow and geomechanical fault-slip analysis. Energy Conv. Man., 47:1798-1807.

Rutqvist, J., Kim, H.-M., Ryu, D.-W., Synn, J.-H., Song, W.-K., 2012. Modeling of coupled thermodynamic and geomechanical performance of underground compressed air energy storage in lined rock caverns. Int J Rock Mech & Min Sci, 52, 71–81.

Samuelson, J., Spiers, C.J., 2012. Fault friction and slip stability not affected by CO2 storage: Evidence from short-term laboratory experiments on North Sea reservoir sandstones and caprocks. Int. J. Greenhouse Gas Control, 11S: S78–S90.

Sibson, R.H., 2003. Brittle-failure controls on maximum sustainable overpressure in different tectonic stress regimes, Bull. Am. Assoc. Petrol. Geol., 87, 901–908.

Starr, J., 2011. Closure Stress Gradient Estimation of the Marcellus Shale from Seismic Data. Society of Exploration Geophysists (SEG) San Antonio 2011 Annual Meeting.

Tutuncu, A., 2010. Anisotropy, compaction and dispersion characteristics of reservoir and seal shales. In proceedings of the 44th US Rock Mechanics Symposium, Salt Lake City, UT June 27–30, 2010.

US DOE, 2009. Modern shale gas development in the United States: A primer. U.S. Department of Energy Office of Fossil Energy and National Energy Technology Laboratory. April 2009.

Wong, T.-F., Ko, S.-C., Olgaard, D.L., 1997. Generation and maintenance of pore pressure excess in a dehydrating system, 2. Theoretical analysis. J. Geophys. Res., 102, B1, 841-852.

Zoback, M.D. 2007. Reservoir Geomechanics. Cambridge University Press, Cambridge, UK.

Zoback, M., Kitasei, S., and Copithorne, B., 2010. Addressing the Environmental Risks from Shale Gas Development Briefing Paper 1. Natural Gas and Sustainable Energy Initiative, Worldwatch Institute, Washington, July 2010 (http://www.worldwatch.org).

Zoback, M.D., Kohli, A., Das, I., McClure, D., 2012. The importance of slow slip on faults during hydraulic fracturing stimulation of shale gas reservoirs. Paper presented at the Americas Unconventional Resources Conference, Pittsburgh, Pennsylvania, USA, 5–7 June 2012.

Table 1. Frequency and occurrence of earthquakes (source Us Geological Survey, http://earthquake.usgs.gov/earthquakes/eqarchives/year/eqstats.php).

Magnitude	Average Annually	Comment
8 and higher	1	Based on observations since 1900
7 - 7.9	15	
6 - 6.9	134	Based on observations since 1990
5 - 5.9	1319	
4 - 4.9	13,000	Estimated
3 - 3.9	130,000	
2 - 2.9	1,300,000	

Table 2. Rock characteristics considered in the basic simulations.

Parameters	**Shale**	**Fault1 (soft without cohesion)**	**Fault2 (stiff with cohesion)**
Young's modulus, E (GPa)	30	5	30
Poisson's ratio, ν (-)	0.2	0.25	0.2
Rock density, ρ_s (kg/m^3)	2700	2700	2700
Biot's coefficient, α (-)	1	1	1
Matrix friction angle φ (°)	-	75	75
Matrix cohesion (MPa)	-	-	6
Matrix tensile strenght (MPa)	-	-	0
Joint peak friction angle, φ (°)	-	31	31
Joint residual friction angle φ (°)	-	11	11
Joint cohesion (MPa)	-	0	3
Joint residual cohesion		0	0
Joint tensile strength (MPa)	-	0	0
Dilation angle, ψ (°)	-	10	10
Porosity, ϕ (-)	0.01	0.01	0.01
Permeability, k (m^2)	10^{-19}	10^{-19} - 10^{-16}	10^{-19} - 10^{-17}

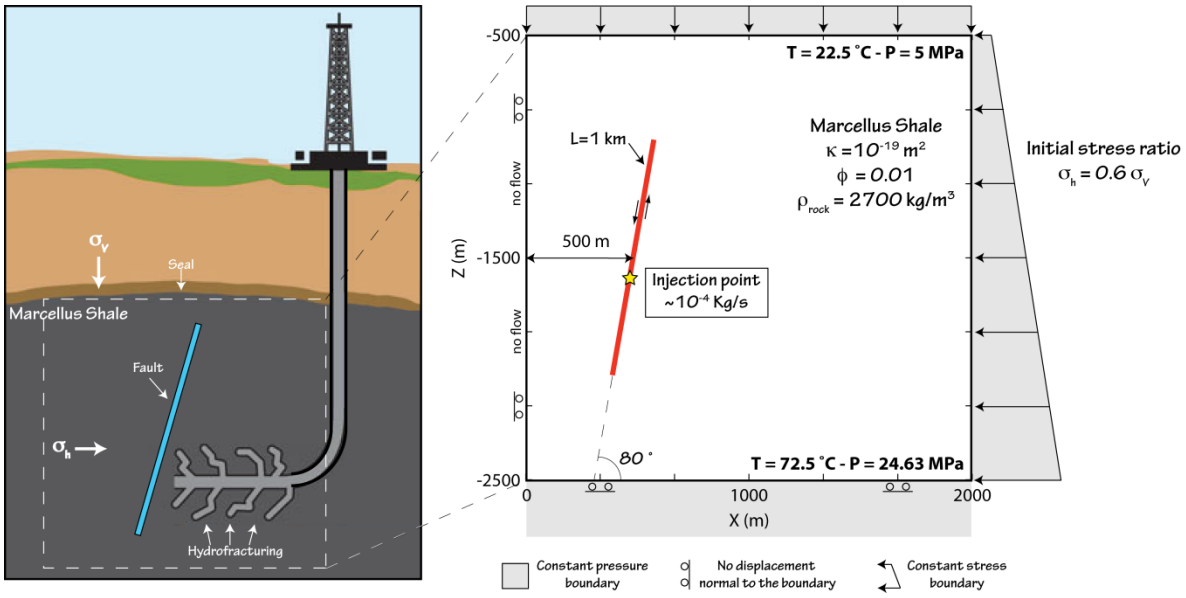

Figure 1. Modeling of reactivation of a minor subvertical fault as a result of nearby shale gas fracturing operation. (a) Schematics and (b) numerical model domain with initial and boundary conditions.

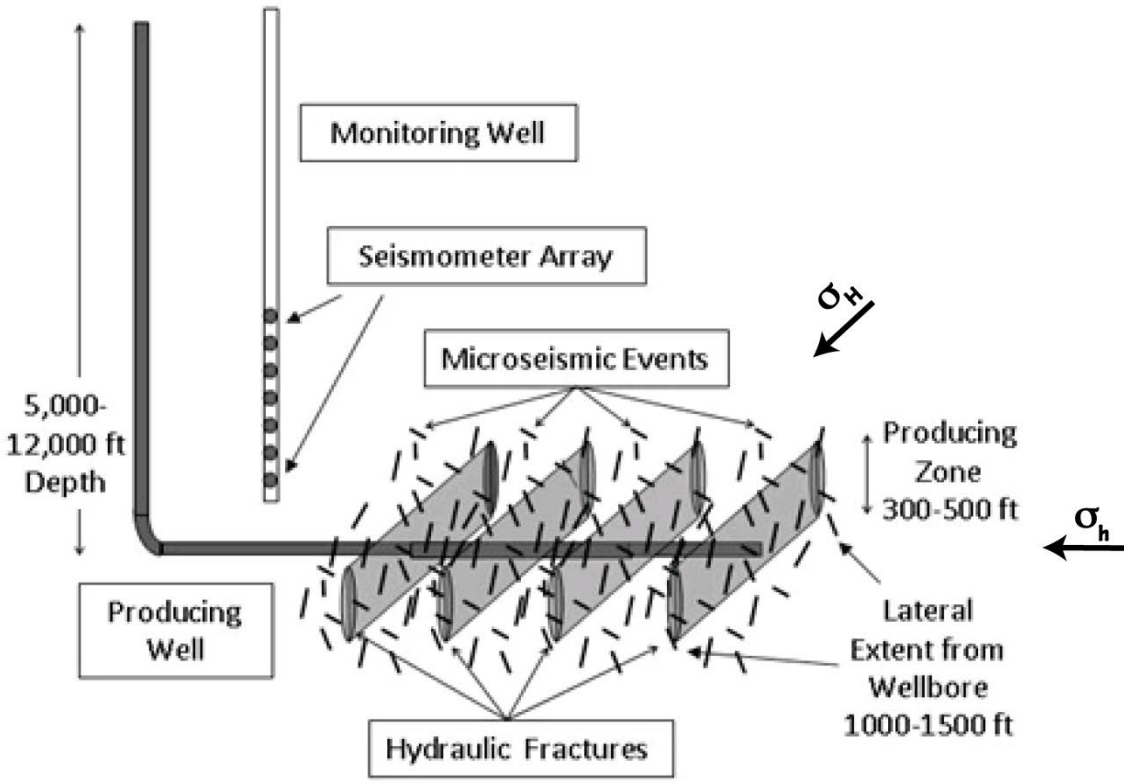

Figure 2. Typical configuration of hydro-fracturing operation along a horiziontal well ((http://shalegaswiki.com/index.php/Hydraulic_fracturing). In this modeling we consider one such hydraulic fracturing extending up and connecting with a fault.

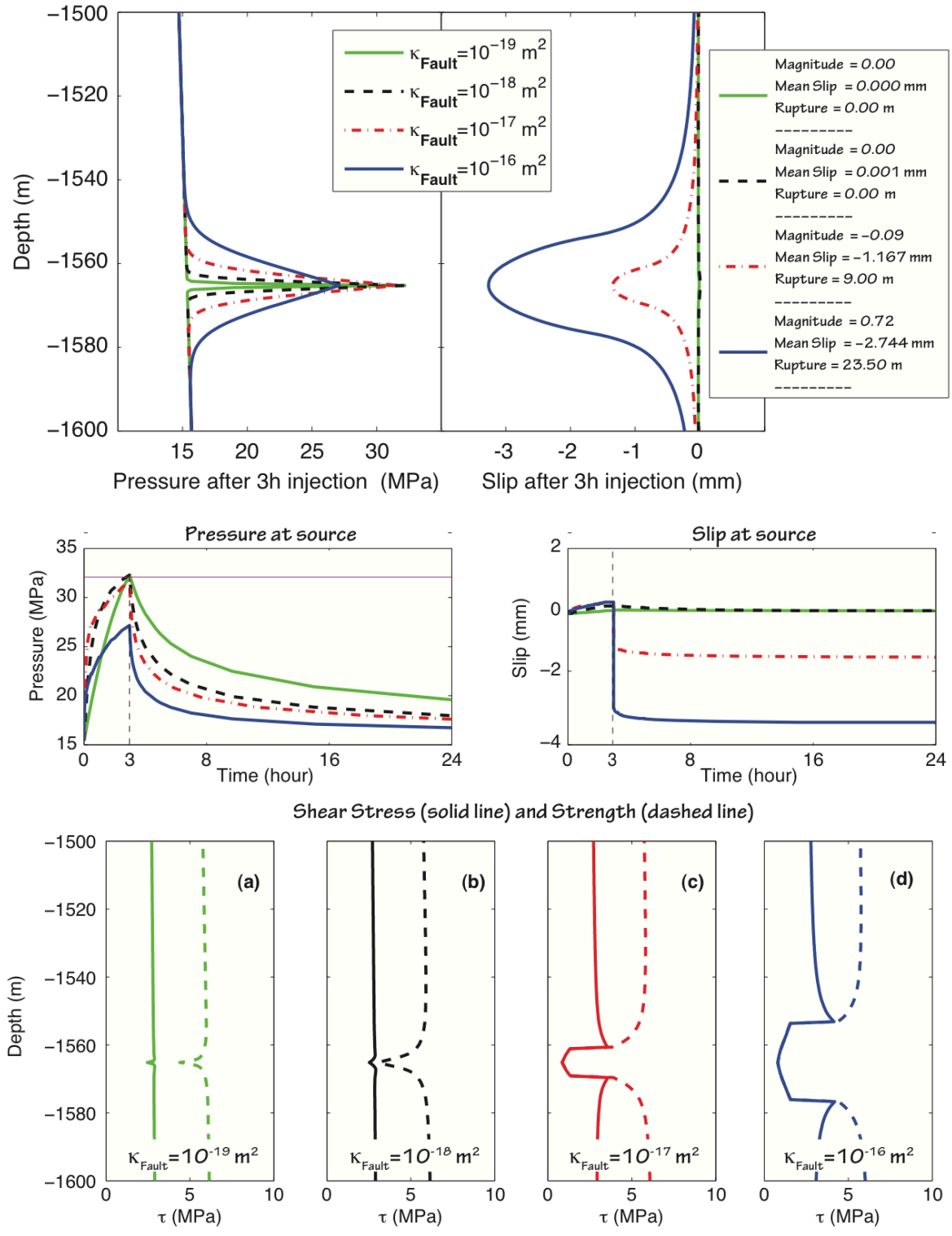

Figure 3. Simulated induced-induced fault reactivation under similar rates of pressure increase with variation of initial (pre-injection) fault permeability.

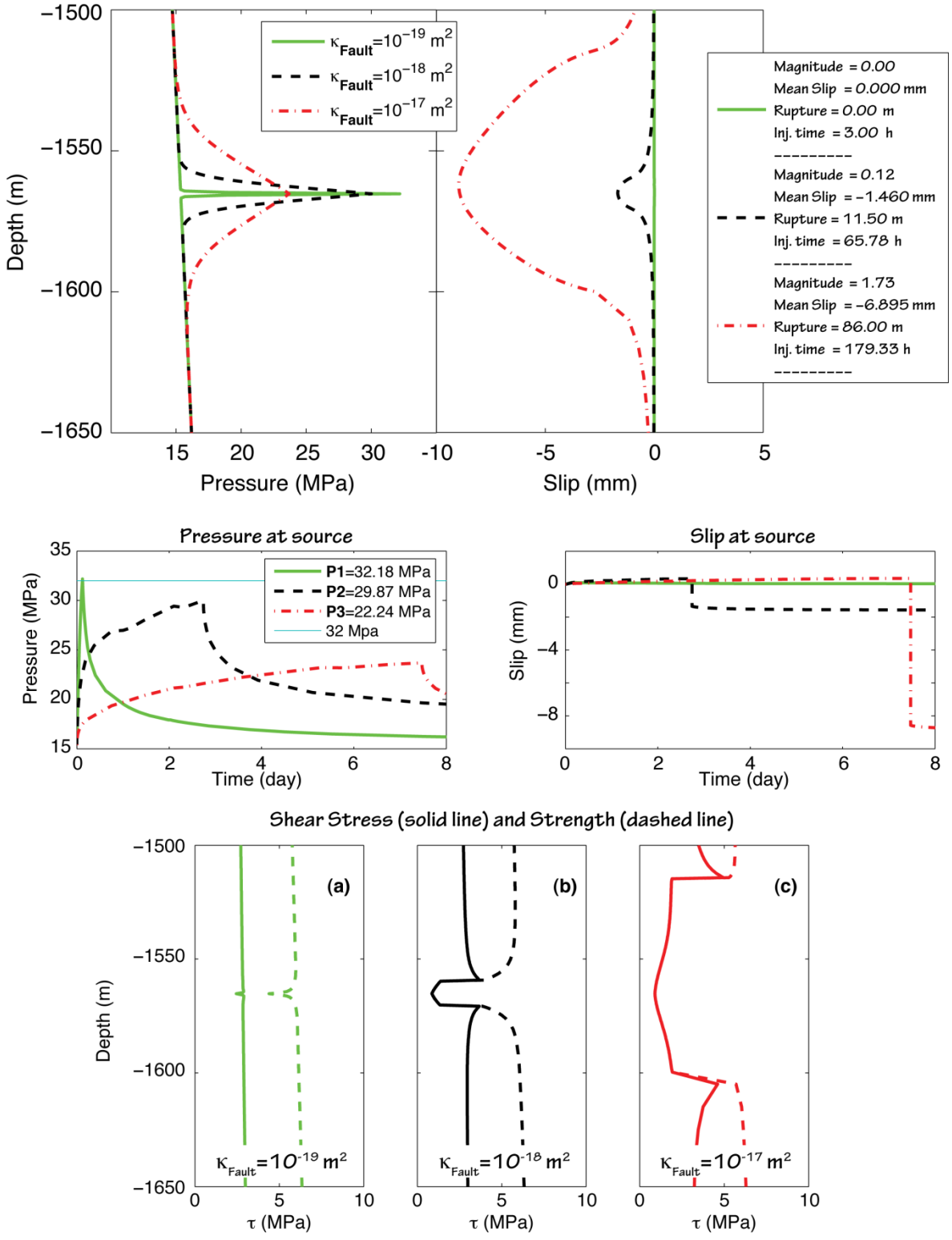

Figure 4. Simulated induced-induced fault reactivation under constant injection rate with variation of initial (pre-injection) fault permeability.

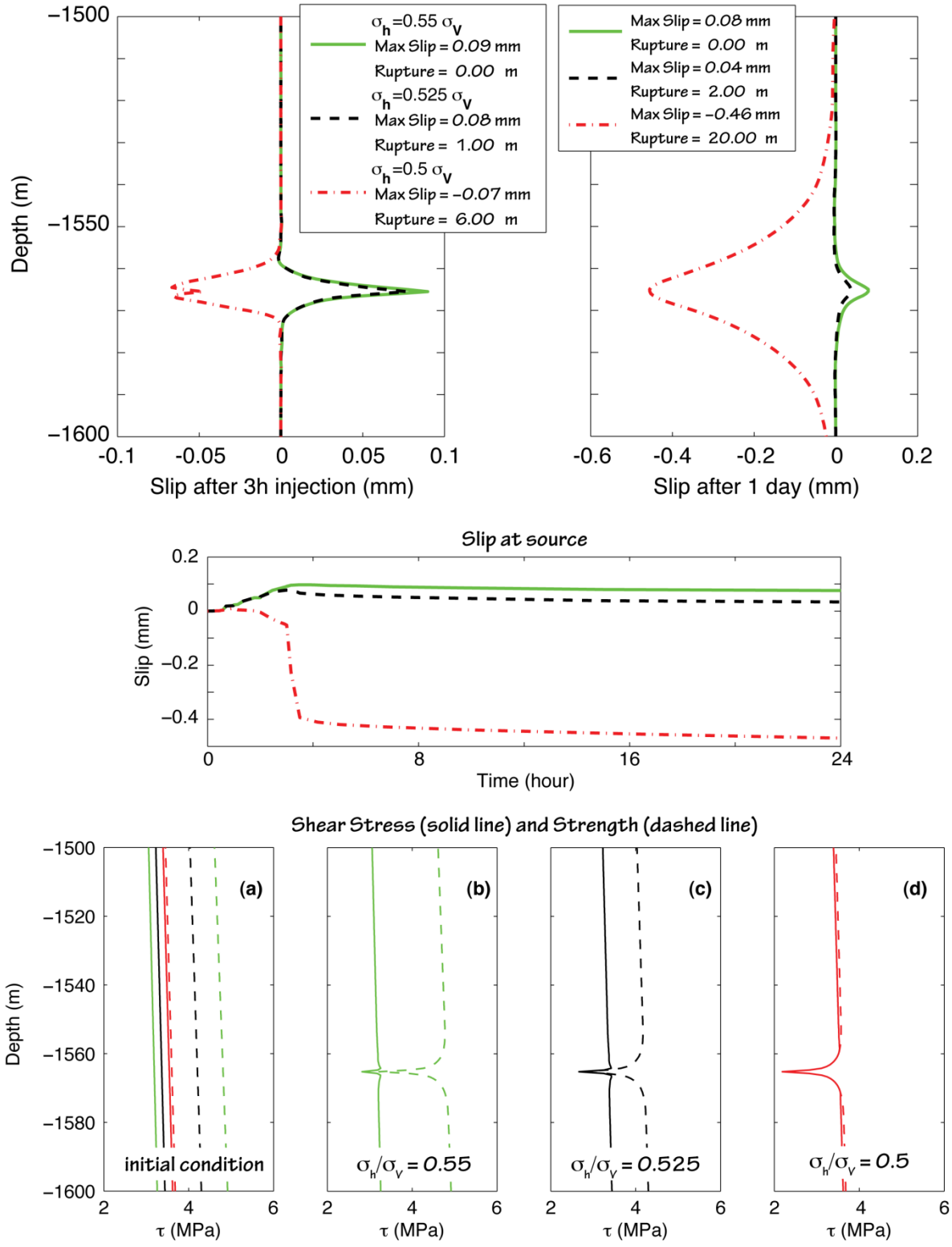

Figure 5. Injection-induced aseismic reactivation along an impermeable fault (k = 1×10^{-19} m^2) at different horizontal over vertical stress ratios.

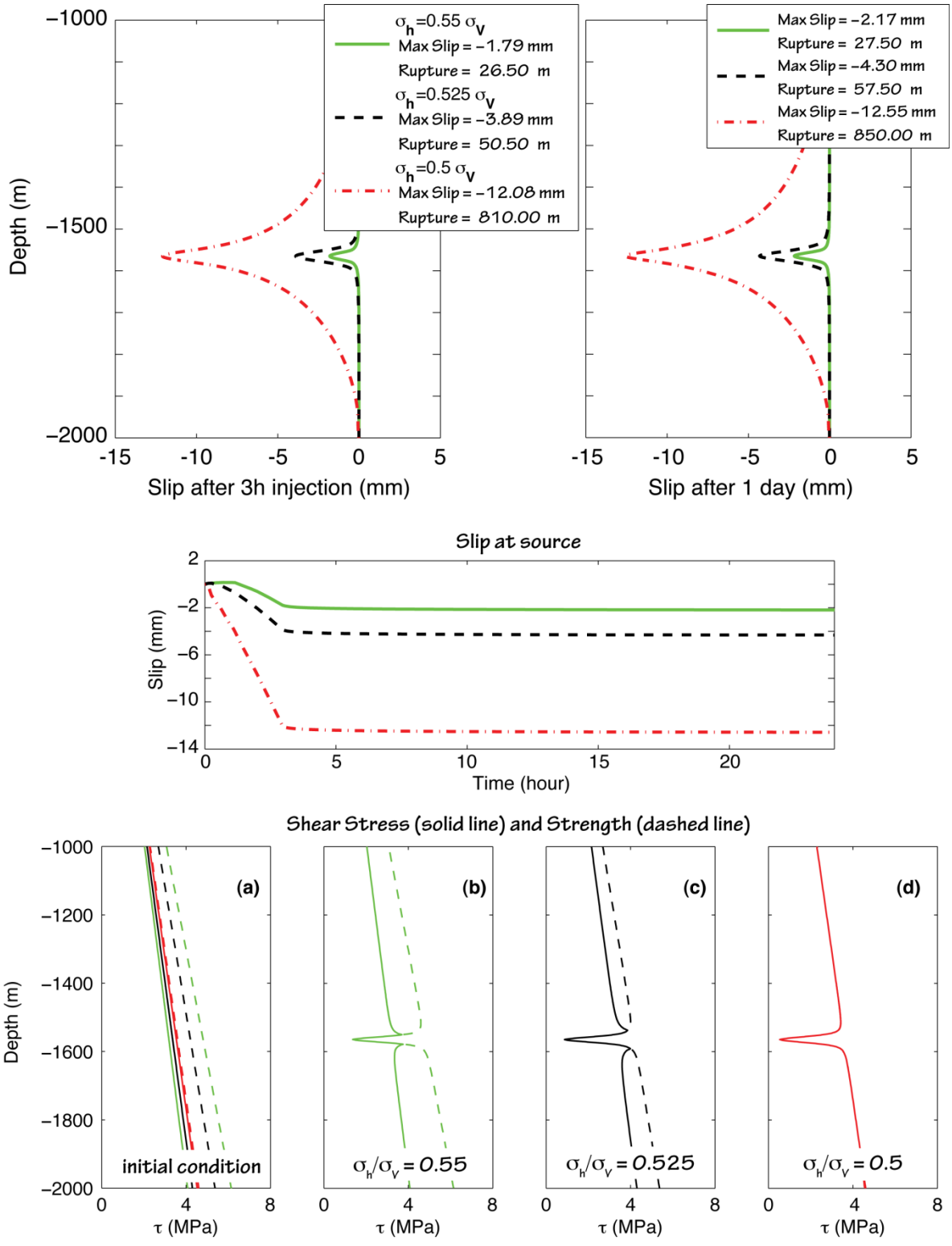

Figure 6. Injection-induced aseismic reactivation along a permeable fault (k = 1×10^{-16} m^2) at different horizontal over vertical stress ratios.

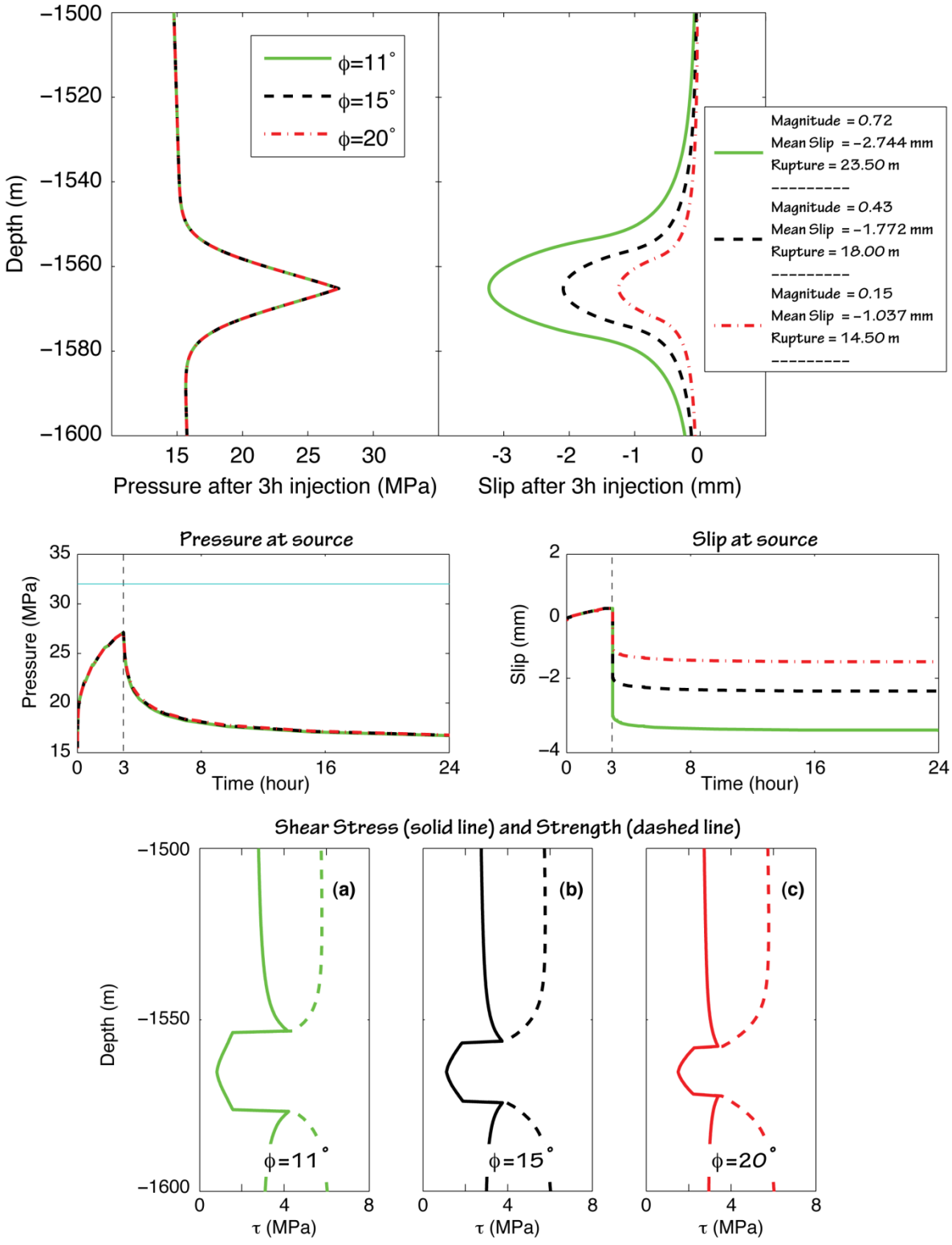

Figure 7. Parameter study showing the impact of the residual coefficient of friction on the rupture length and seismic magnitude.

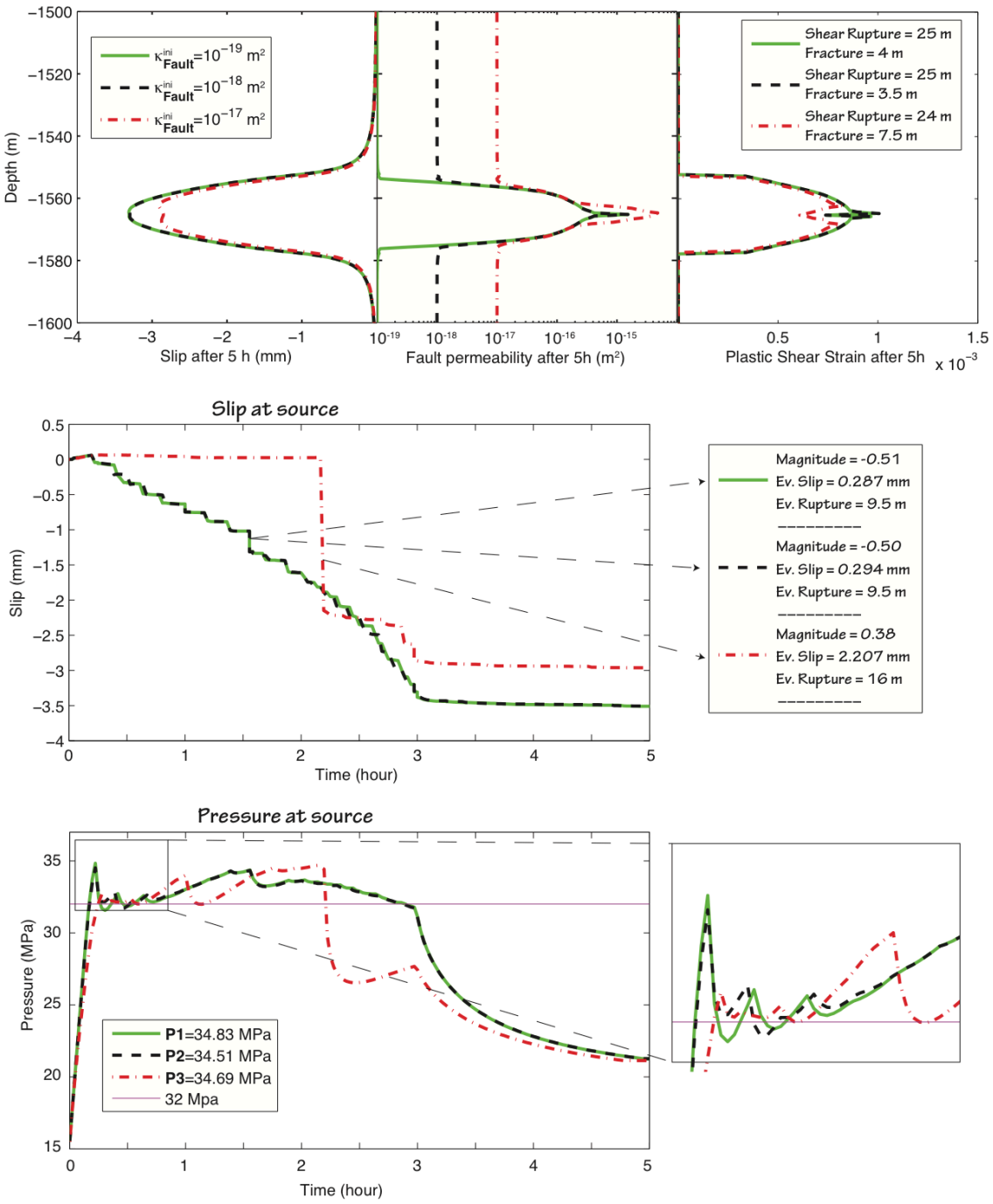

Figure 8. Simulated injection-induced hydraulic fracturing and fault reactivation under similar rates of pressure increase with variation of initial (pre-injection) fault permeability.